


EXPRESS LETTER

Open Access



# Simple empirical method for estimating lava-effusion rate using nighttime Himawari-8 1.6- $\mu\text{m}$ infrared images

Takayuki Kaneko<sup>1\*</sup> , Atsushi Yasuda<sup>1</sup> and Toshitsugu Fujii<sup>2</sup>

## Abstract

The effusion rate of lava is one of the most important eruption parameters, as it is closely related to the migration process of magma underground and on the surface, such as changes in lava flow direction or formation of new effusing vents. Establishment of a continuous and rapid estimation method has been an issue in volcano research as well as disaster prevention planning. For effusive eruptions of low-viscosity lava, we examined the relationship between the nighttime spectral radiance in the 1.6- $\mu\text{m}$  band of the Himawari-8 satellite (R1.6Mx: the pixel value showing the maximum radiance in the heat source area) and the effusion rate using data from the 2017 Nishinoshima activity. Our analysis confirmed that there was a high positive correlation between these two parameters. Based on the linear-regression equation obtained here ( $Y = 0.47X$ , where  $Y$  is an effusion rate of  $10^6 \text{ m}^3 \text{ day}^{-1}$  and  $X$  is an R1.6Mx of  $10^6 \text{ W m}^{-2} \text{ sr}^{-1} \text{ m}^{-1}$ ), we can estimate the lava-effusion rate from the observation data of Himawari-8 via a simple calculation. Data from the 2015 Raung activity—an effusive eruption of low-viscosity lava—were arranged along the extension of this regression line, which suggests that the relationship is applicable up to a level of  $\sim 2 \times 10^6 \text{ m}^3 \text{ day}^{-1}$ . We applied this method to the December 2019 Nishinoshima activity and obtained an effusion rate of  $0.50 \times 10^6 \text{ m}^3 \text{ day}^{-1}$  for the initial stage. We also calculated the effusion rate for the same period based on a topographic method, and verified that the obtained value,  $0.48 \times 10^6 \text{ m}^3 \text{ day}^{-1}$ , agreed with the estimation using the Himawari-8 data. Further, for Nishinoshima, we simulated the extent of hazard areas from the initial lava flow and compared cases using the effusion rate obtained here and the value corresponding to the average effusion rate for the 2013–2015 eruptions. The former distribution was close to the actual distribution, while the latter was much smaller. By combining this effusion-rate estimation method with real-time observations by Himawari-8 and lava-flow simulation software, we can build a rapid and precise prediction system for volcano hazard areas.

**Keywords:** Himawari-8, Volcanoes, Effusion rate, Lava, Remote sensing, Infrared

## Introduction

It has been a vital issue to develop a method for continuous and quick estimation of the discharge rate of lava, to promote volcano research and disaster prevention planning. The discharge rate is one of the prime parameters that affects various aspects of eruptive activities. In effusive eruptions, the discharge rate is closely related to the

length of lava flows (Walker 1973) and is also a critical input parameter that influences the results of lava-flow simulations (e.g., Ishihara et al. 1990; Miyamoto and Sasaki 1998). There are two ways to describe the discharge rate for effusive eruptions (Wadge 1981): the “eruption rate” is the average discharge rate throughout the activity period, and the “effusion rate” is the instantaneous discharge rate, which changes over the course of the activity. Notably, knowing the effusion rate is essential because it is closely related to the migration process of magma underground (Wadge 1981), as well as surface phenomena, including short-term events such as

\*Correspondence: kaneko@eri.u-tokyo.ac.jp

<sup>1</sup> Earthquake Research Institute, The University of Tokyo, 1-1-1 Yayoi, Bunkyo-ku, Tokyo 113-0032, Japan

Full list of author information is available at the end of the article

the growth pattern of lava domes (e.g., exogenous versus endogenous growth; Nakada et al. 1995), in addition to changes in the flow direction of lava or the formation of new effusing vents (Kaneko et al. 2019b).

Despite the importance of the effusion rate, its measurement is not straightforward. To obtain precise information on variations in the effusion rate, we need to make very complex topographic measurements over short intervals (e.g., Harris et al. 2007; Maeno et al. 2016; Nakada et al. 1999; Swanson et al. 1987). One method estimates the discharge rate based on a heat budget between heat supplied to the active flow unit by advection of lava and the heat loss from the flow surfaces (Coppola et al. 2013, 2019; Harris et al. 1997, 2007; Harris and Bologna 2009; Pieri and Bologna 1986; Wright et al. 2001). The problems with these methods are that various assumptions are required to estimate the discharge rate from low-resolution thermal infrared (TIR, e.g., 11  $\mu\text{m}$ ) or mid-wave infrared (MIR, e.g., 4.0  $\mu\text{m}$ ) satellite images, as discussed below, and the obtained discharge rate is a time-averaged value over a given period (time-averaged discharge rate) rather than an instantaneous value, that is, the effusion rate (Coppola et al. 2013, 2019; Harris et al. 2007; Harris and Bologna 2009; Wright et al. 2001). In the method proposed by Harris et al. (1997, 2007), Harris and Bologna (2009), and Wright et al. (2001), surface temperature of the active lava is regarded as uniform ( $T_e$  effective radiation temperature). As  $T_e$  is unknown, given a reasonable minimum–maximum temperature range (e.g., 100–500  $^{\circ}\text{C}$ ), for several values of  $T_e$  within this range, areas of active lava are calculated from the radiance values in the TIR images. Then, time-averaged discharge rates are calculated from the relationship between time-averaged discharge rates and the area of active lava (Pieri and Bologna 1986). In this method, however, the surface temperature ( $T_e$ ) of the active lava is assumed to be uniform, which is unrealistic for typical lava flows (Dragoni and Tallarico 2009). The assumption of a range of  $T_e$  values also produces a wide range of volume fluxes (time-averaged discharge rates). Further, the empirical parameters relating to the rheological properties, the magma temperature, and the slope inclination need to be considered on a case-by-case basis (Harris et al. 2007; Harris and Bologna 2009; Wright et al. 2001). These terms can be possible error factors. In contrast, Coppola et al. (2013, 2019) estimated the time-averaged discharge rate from the volcanic radiative power using MIR images by adopting the method for calculation of fire radiative energy used in the studies of wildfires (Wooster et al. 2003), coupled with an empirical parameter—radiant density. Calculation of the fire radiative energy is based on the fact that the ratio of total power emitted over all wavelengths to the power emitted at  $\sim 4.0 \mu\text{m}$  is almost

constant in a temperature range of  $\sim 330$ – $1230$   $^{\circ}\text{C}$ . Unlike wildfires, however, a certain amount of the area of an active lava surface is considered to be below  $330$   $^{\circ}\text{C}$ , which can potentially cause some errors (Harris 2013).

We focused on the thermal anomaly in the  $1.6\text{-}\mu\text{m}$  shortwave infrared (SWIR) images from the Himawari-8 satellite for the estimation. It is reported that in the effusive activity, thermal anomalies in the  $1.6\text{-}\mu\text{m}$  satellite images show a temporal variation similar to that for the lava-effusion rate estimated by the topographic method—a positive correlation—in the 1991–1994 Unzen (Kaneko et al. 2002; Kaneko and Wooster 1999; Wooster and Kaneko 1998), the 2015 Raung (Kaneko et al. 2019a), and the 2017 Nishinoshima (Kaneko et al. 2019b) activities. If we can obtain a regression equation with sufficient accuracy between these two parameters, the effusion rate can be estimated by the satellite observation.

The method using a regression equation can simply calculate effusion rates without assuming particular temperatures or unconfirmed relationships. Especially, when similar activities continue in a volcano, once that activity's regression equation is obtained, we can estimate effusion rate from the spectral radiance showing a thermal anomaly rather accurately, because differences in various factors, such as the magma temperature, the rheological properties, the content of crystals, the content and shape of bubbles (Llewellyn and Manga 2005), or the emissivity (Rogic et al. 2019) are considered to be minimized.

As the  $1.6\text{-}\mu\text{m}$  band is preferentially sensitive to high-temperature materials, such as incandescent lava (Wooster and Kaneko 1998; Wooster and Rothery 1997), the anomaly is thought to reflect the effusion of high-temperature lava near the vent, which is closely related to the *instantaneous* effusion rate (Kaneko et al. 2002, 2019a). By using the  $1.6\text{-}\mu\text{m}$  band of Himawari-8, thus, we can obtain high-density temporal variations in the lava-effusion rate, including short-term events, by taking advantage of the high repetition rate of Himawari-8 observations. Such observational data cannot be obtained by other methods and are essential for understanding eruptive processes. The time-averaged discharge rate, determined by the method using TIR or MIR images, is not ideal for observing short-term phenomena ( $\sim 1$  h).

In this study, to estimate the effusion rate for low-viscosity lava, we developed a simple empirical method based on the relationship between the lava-effusion rate and the thermal anomaly in the  $1.6\text{-}\mu\text{m}$  band measured by Himawari-8. We collected pairs of these parameters for the 2017 Nishinoshima activity and used them to obtain a regression equation. Then, this method was applied to the initial stage of the December 2019 Nishinoshima activity as a test case. The estimated effusion rate was verified by comparison with the value

determined by the topographic method. Further, we used simulation software for lava flows to evaluate how the estimated effusion rate could improve the prediction of the location of hazardous areas.

## Methodology

### Himawari-8 satellite

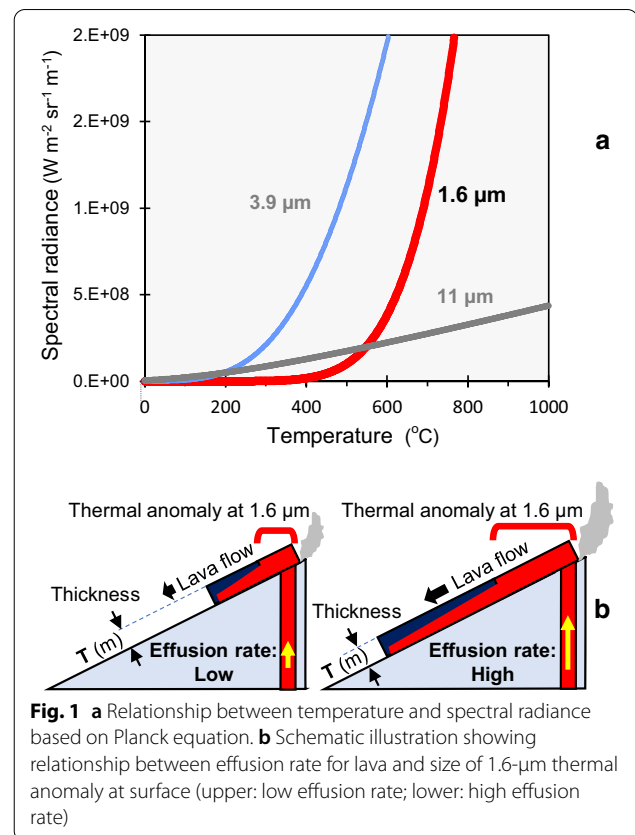
Himawari-8, a meteorological satellite operated by the Japan Meteorological Agency (JMA), is in a geostationary orbit about 35,786 km above the equator at a longitude of 140.7°E (JMA 2017). The satellite can perform measurements in 16 wavebands from the visible to the thermal infrared regions. It can observe a full disk at 10-min intervals. The pixel size in the SWIR to the TIR bands is about 2 km × 2 km in the equatorial region (JMA 2017). Because of the large pixel size, an eruption center—an effusing vent and the adjacent region—is usually contained within a single pixel. In this study, we used nighttime images in the 1.6-μm band to avoid the effects of reflected sunlight. A vast number of active volcanoes, such as those in the Asia–Pacific region, are located within the observation area of Himawari-8, and some of these occasionally undergo disastrous eruptions.

### Characteristics of the 1.6-μm band

In the relationship between the temperature and the spectral radiance specified by the Planck equation, although the spectral radiance at 1.6 μm is low (close to the background) in the temperature range below ~300–400 °C, it becomes orders of magnitude greater at higher temperatures (Fig. 1a). Therefore, the 1.6-μm band provides a sensitive indication of the temperature and size of high-temperature areas within a pixel, such as those due to incandescent lava, but is insensitive to medium and low-temperature areas (Wooster and Kaneko 1998; Wooster and Rothery 1997). This is in contrast to other bands, such as the 4.0- and 11-μm bands in the MIR and TIR regions.

### Assumed processes for lava effusion

In an effusive eruption of low-viscosity lava, a thermal anomaly extends over the lava surface from the effusing vent. The surface temperature is close to the magmatic temperature (up to ~1200 °C) at the effusion point. However, immediately after effusion, heat radiation at the surface quickly reduces the temperature (Kilburn et al. 1995; Miyamoto and Sasaki 1998; Pieri and Bologna 1986). At this time, a solidified layer begins to form on the surface of the lava flow (Kilburn et al. 1995; Miyamoto and Sasaki 1998; Pieri and Bologna 1986). Due to its low thermal conductivity, the solidified surface temperature decreases exponentially with time (Harris and



Bologna 2009), even when the molten lava underneath is much hotter. It is estimated that the surface temperature of lava flow falls below 300–400 °C within a few hours after effusion (Yamashita and Miyamoto 2009). If the effusion temperature (i.e., magmatic temperature) and the lava-flow thickness adjacent to the effusing vent are considered nearly constant throughout the activity regardless of the effusion rate, the size of the high-temperature area (> ~300–400 °C) varies in proportion to the effusion rate; thus, the 1.6-μm spectral radiance also changes in the same manner (Fig. 1b). Compared with the short time scale for cooling of the high-temperature area observed at 1.6 μm (a few hours), the time scale for changes in the effusion rate is generally long (greater than a day). Therefore, the effusion rate we obtain from observations with the 1.6-μm band images is considered mostly to reflect the effusion rate at the time of observation, except just after an acute change. Lava effusion is basically assumed to be quasi-steady, as with the methods using the TIR and MIR images (e.g., Dragoni and Tallarico 2009). Although extra cooling is expected in eruptions with discharge rates higher than 100 m<sup>3</sup> s<sup>-1</sup>, due to self-induced convection currents (Garel et al. 2013), we do not deal with such large discharge rates here.

### Data preparation

Data for the lava-effusion rate and the thermal anomaly at 1.6  $\mu\text{m}$  were carefully selected for two events: the 2017 Nishinoshima activity (Kaneko et al. 2019b) and the 2015 Raung activity (Kaneko et al. 2019a). Both activities were dominated by effusion of low-viscosity lava accompanied by Strombolian eruptions. The effusion temperature of the lava was estimated to be 1060–1090  $^{\circ}\text{C}$  for the 2013–2015 Nishinoshima activity (Maeno et al. 2016), while no data have been reported for the 2015 Raung activity. In these analyses, the volume of the pyroclastic cone was taken as the dense-rock equivalent (DRE), and as an indicator of the thermal anomaly, R1.6Mx—the pixel value showing the highest spectral radiance at 1.6  $\mu\text{m}$  (Kaneko et al. 2018a)—was used. Further, corrections for atmospheric effects, emissivity and stray solar light (Kaneko et al. 2018b) were also made. To obtain reliable data, we selected the values of R1.6Mx and effusion rate during periods when topographic measurement points were dense, or variations in these parameters were nearly constant. In this process, the maximum value of R1.6Mx each night was adopted to avoid or minimize the influence of partial coverage by small clouds and/or plumes over the high-temperature areas within the pixel, and when the high-temperature area was occasionally located on the boundary of multiple pixels in the images.

### Analytical methods for initial stage of December 2019 Nishinoshima activity

In the analysis of the December 2019 Nishinoshima activity using this simple empirical method, the same processing procedures and corrections described above were applied. Atmospheric correction was performed with MODTRAN 3.7 (Berk et al. 1989), for which a subtropical model (winter, altitude of 50 m) was adopted; the transmittance at 1.6  $\mu\text{m}$ ,  $\varepsilon_{1.6}$ , was estimated to be 0.89. The emissivity at 1.6  $\mu\text{m}$ ,  $\tau_{1.6}$ , was assumed to be 0.95 with reference to that in the TIR region (Harris 2013; Walter and Salisbury 1989). The atmospherically and emissivity-corrected radiance (e.g., Harris 2013), R1.6Mx, was calculated based on the following equation from the stray solar light-corrected radiance (Kaneko et al. 2018b), R1.6Mx<sub>vg\_obs</sub>:

$$\text{R1.6Mx} = \text{R1.6Mx}_{\text{vg\_obs}} / (\tau_{1.6}\varepsilon_{1.6}). \quad (1)$$

### Results: relationship between lava-effusion rate and spectral radiance at 1.6 $\mu\text{m}$

The obtained values for the effusion rate and spectral radiance at 1.6  $\mu\text{m}$  (R1.6Mx) are given in Table 1, and their relationship is shown in Fig. 2. The plots for the 2017 Nishinoshima activity show a nearly linear relationship (Fig. 2a). The correlation between R1.6Mx and the

**Table 1** Extracted values for effusion rate for lava and spectral radiance at 1.6  $\mu\text{m}$  (R1.6Mx) for 2017 Nishinoshima activity (Kaneko et al., 2019b) and 2015 Raung activity (Kaneko et al., 2019a)

Observation date	1.6- $\mu\text{m}$ radiance ( $10^6 \text{ W m}^{-2} \text{ sr}^{-1} \text{ m}^{-1}$ )	Effusion rate of lava ( $10^6 \text{ m}^3 \text{ day}^{-1}$ )
2015 Raung / 23 Jun*	1.18	0.5
2015 Raung / 27 Jul*	2.51	0.79
2015 Raung / 4 Jul*	3.31	1.47
2015 Raung / 15 Jul*	3.18	1.63
2017 Nishinoshima / 23 Apr**	0.71	0.35
2017 Nishinoshima / 8 May**	0.50	0.23
2017 Nishinoshima / 30 Jun**	0.26	0.094
2017 Nishinoshima / 25 Jul**	0.10	0.014

\* Kaneko et al., 2019a, \*\*Kaneko et al., 2019b

effusion rate is very high ( $R^2=0.99$ ). This relationship shows that although they were different in magnitude, the eruption mechanism was similar, that is, effusive eruption of similar low-viscosity lava on a gentle topography. The linear relationship suggests that the size of the high-temperature area near the effusing vent changed in proportion to the increase in the effusion rate as expected. The linearity also shows that the thickness of the lava flow was roughly unchanged regardless of the effusion rate. The data from the 2017 Nishinoshima activity were used to apply a regression line through the origin and obtain the following equation (Fig. 2a):

$$Y = 0.47X \quad (2)$$

where  $Y$  is the effusion rate ( $10^6 \text{ m}^3 \text{ day}^{-1}$ ) and  $X$  is R1.6Mx ( $10^6 \text{ W m}^{-2} \text{ sr}^{-1} \text{ m}^{-1}$ ). Strictly speaking, spattering of incandescent lava fragments in the Strombolian fountaining, incandescent lava partially exposed through cracks in surficial crust layers (Crisp and Bologna 1990), and effusion of new lobes at the front of lava flows (Maeno et al. 2016; Kaneko et al. 2019b) might affect the thermal anomaly at 1.6  $\mu\text{m}$ . However, the high correlation seen in Fig. 2a suggests that these contributions were either relatively small, that they changed in harmony with changes in the effusion rate, or both.

Data from the 2015 Raung activity are plotted together with those from the 2017 Nishinoshima activity in Fig. 2b. The data points for the 2015 Raung activity are arranged along the extension of the regression line obtained from the 2017 Nishinoshima data (Fig. 2b). Based on this relationship and the eruptive characteristics (an effusive eruption with low-viscosity lava), the lava-effusion temperature and viscosity during the 2015 Raung activity are broadly similar to those for the 2017 Nishinoshima



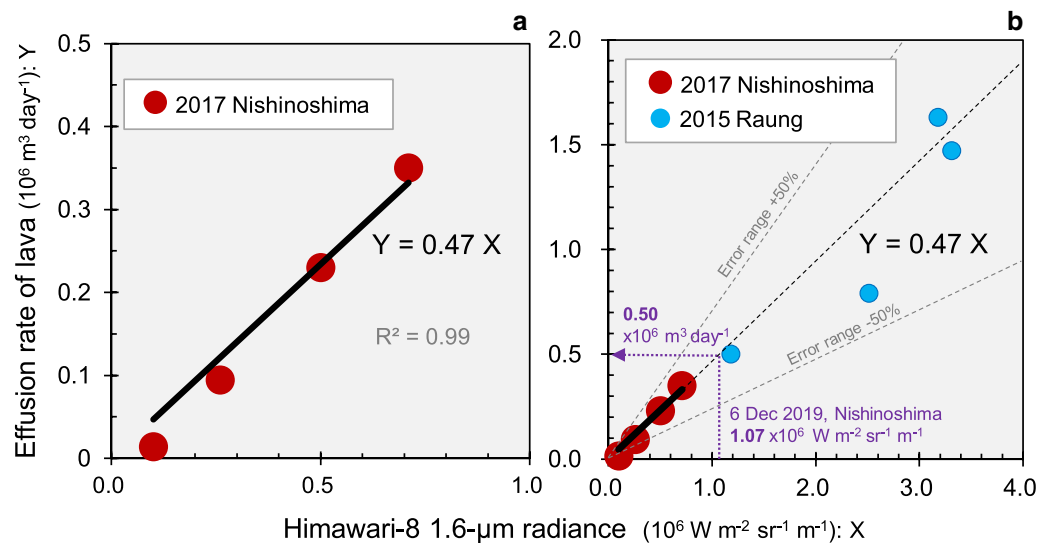


**Fig. 2** Relationship between effusion rate for lava and 1.6-μm radiance. **a** 2017 Nishinoshima activity. **b** 2017 Nishinoshima and 2015 Raung activities. The regression line was obtained from the 2017 Nishinoshima data

activity. Further, these observations suggest that the linear relationship expressed by Eq. (2) is applicable up to an effusion rate of  $\sim 2 \times 10^6 \text{ m}^3 \text{ day}^{-1}$  for lava with physical properties similar to those of the 2017 Nishinoshima activity. If we calculate the regression equation for both plots, the equation  $Y' = 0.44X$  can be obtained.

When the regression equation obtained here is applied to an eruption at a different eruptive stage or volcano, we need to check the similarities of the magma temperature, the rheological properties, and the slope inclination to those in the base equation—that is, that for the 2017 Nishinoshima activity—not just the eruption style. For example, when using Eq. (2), compared to the 2017 Nishinoshima activity, if the magma temperature is higher, the viscosity is lower, or the slope inclination is steeper, then the effusion rate can be over-estimated to be higher than the actual value.

It should be noted that it is not appropriate to apply Eq. (2) in its present form to volcanoes located in marginal regions of the Himawari-8 coverage area (e.g., areas where the satellite zenith angle is larger than  $35\text{--}45^\circ$ ). In these regions, the pixel size is larger than  $2 \text{ km} \times 2 \text{ km}$  (e.g., NASA 2019), so the radiance value will be lower than that in the central region for the same heat source. In addition, due to the low elevation angle of Himawari-8, topographic influences become significant in these areas, and in some rare cases, part of the heat source might be shadowed by the terrain.

Due to the limited amount of data at this stage of the research, it is difficult to evaluate the error range. It might be necessary to allow for an estimated error range

of several tens of percent (Fig. 2b) when we apply Eq. (2) to an arbitrary effusive eruption with low-viscosity lava.

### Test case: application to initial stage of December 2019 Nishinoshima activity

The proposed method was applied to Nishinoshima to estimate the effusion rate of the activity that resumed on 4 December 2019. Nishinoshima is an uninhabited remote island in the Pacific Ocean about 1,000 km south of Tokyo. The eruption style was basically similar to that for the 2013–2015, 2017, and 2018 Nishinoshima activities—effusion of low-viscosity lava (Kaneko et al. 2019b; Maeno et al. 2016, 2018). The eruption that started in 2019 continued for approximately 9 months.

Figure 3 shows the observation results by Himawari-8 from 4 to 6 December, the initial stage of the activity. After 5 December, a constant level of R1.6Mx can be seen, except for during a period of cloud cover. A nearly constant thermal anomaly is one of the characteristics of effusive eruption of low-viscosity lava (Kaneko et al. 2018a).

The highest value of the nighttime R1.6Mx between 5 and 6 December was  $1.07 \times 10^6 \text{ W m}^{-2} \text{ sr}^{-1} \text{ m}^{-1}$  at about 5:00 JST on the 6th. Substituting this value into Eq. (2) yields  $0.50 \times 10^6 \text{ m}^3 \text{ day}^{-1}$  as the effusion rate. This effusion rate is more than two times higher than the average value for the 2013–2015 Nishinoshima activity ( $\sim 0.20 \times 10^6 \text{ m}^3 \text{ day}^{-1}$ ; Maeno et al. 2016). If we use the equation  $Y' = 0.44X$ , then  $0.47 \times 10^6 \text{ m}^3 \text{ day}^{-1}$  is obtained as the effusion rate—the difference from the value using Eq. (2) is very small (several per cent).

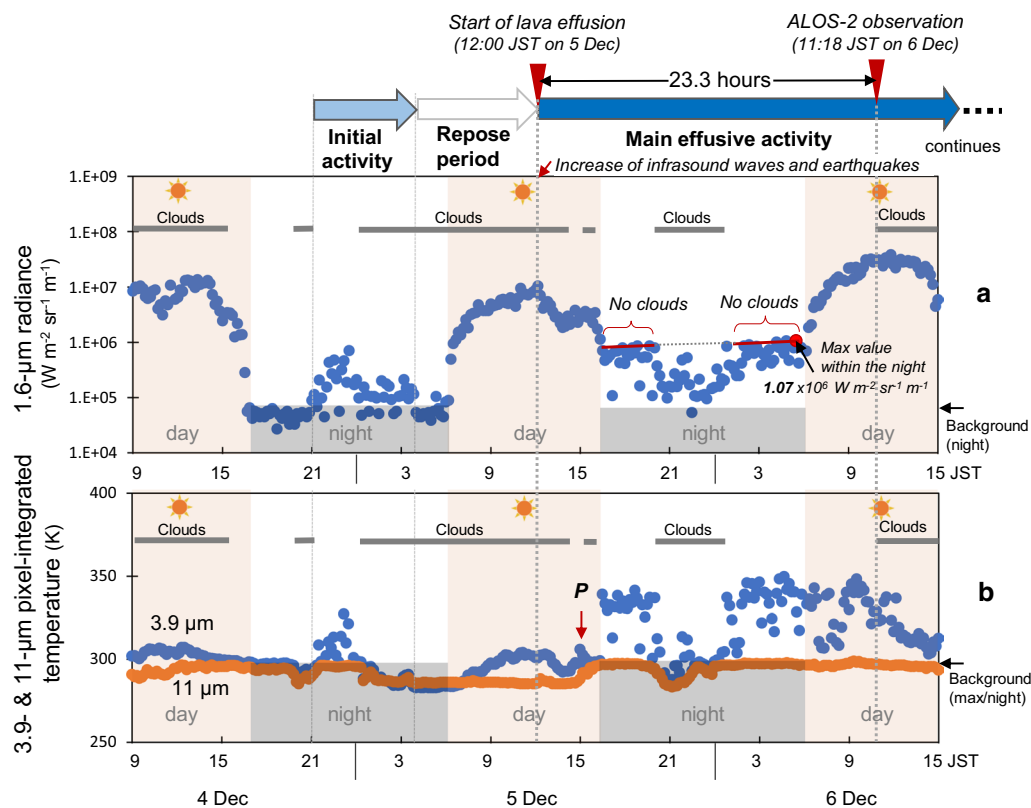


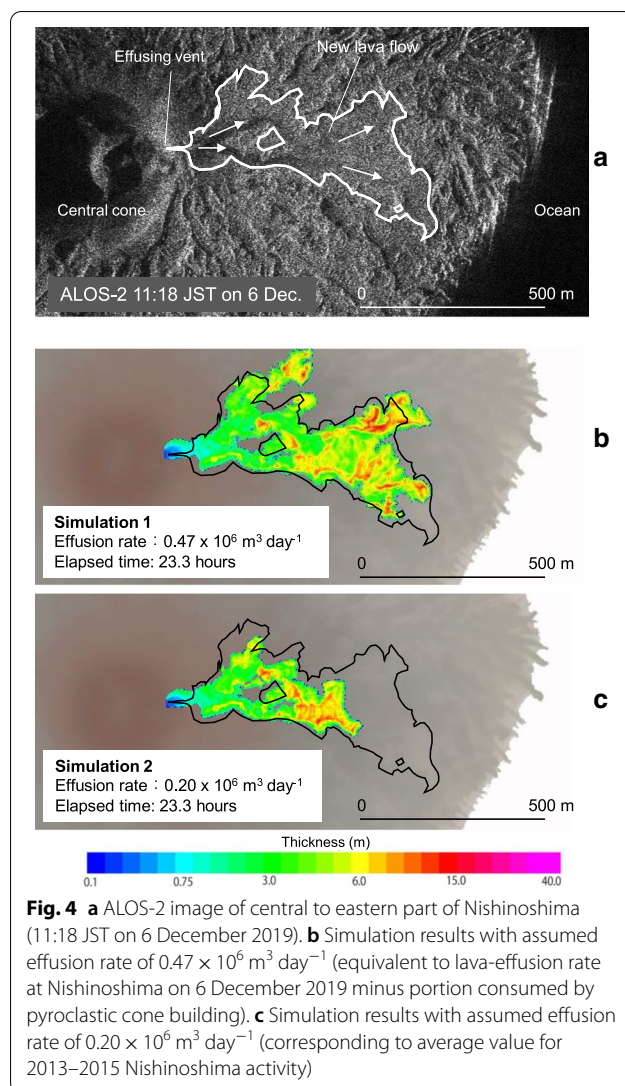
**Fig. 3** a. Time-series variation of 1.6- $\mu\text{m}$  radiance at Nishinoshima between 4 and 6 December 2019. Details of the correction method are described in the main text (and also in Kaneko et al. 2019b). b. Time-series variations of 3.9- $\mu\text{m}$  and 11- $\mu\text{m}$  pixel-integrated temperature at Nishinoshima between 4 and 6 December 2019. The same correction method as that used in Kaneko et al. (2019b) was adopted for the 3.9- $\mu\text{m}$  and 11- $\mu\text{m}$  pixel-integrated temperature ( $\epsilon_{3.9}, 0.95$ ;  $\tau_{3.9}, 0.89$ ;  $\epsilon_{11}, 0.95$ ;  $\tau_{11}, 0.96$ ; upwelling atmospheric radiance at 11  $\mu\text{m}$ ,  $142,000 \text{ W m}^{-2} \text{ sr}^{-1} \text{ m}^{-1}$ )

Through the method presented here, in December 2019, we could identify a high effusion rate at Nishinoshima ( $0.50 \times 10^6 \text{ m}^3 \text{ day}^{-1}$ ), and could determine that this activity was not just a short-term event, but rather a full-scale activity that actually continued until August 2020. Based on this information, we could plan the following observation projects, even when very little observation data had been obtained.

#### Verification using topographic measurement

Figure 4a shows an Advanced Land Observing Satellite 2 (ALOS-2) image obtained at 11:18 JST on 6 December. We can recognize a broad lava flow consisting of a single flow unit flowing to the east from the eastern base of the pyroclastic cone, which is the first lava flow in this activity. These topographic features are similar to those observed during the periods of high lava-effusion rate in the 2013–2015 and 2017 Nishinoshima activities (Kaneko et al. 2019b; Maeno et al. 2016). The distribution area of this lava flow was measured to be about  $130,000 \text{ m}^2$ . According to a landing and survey conducted in 2016,

the thickness of the new lava flow on the flat plain of the basement (Old Nishinoshima) was reported to be 3–5 m at the tip (Maeno et al. 2017); the average thickness of the entire lava flow would be slightly below the middle of this range. Here, we assumed that the thickness was 3.5 m, which resulted in a volume estimate of  $455,000 \text{ m}^3$ . Assuming that the volume of spattered material around the pyroclastic cone accounted for 7% of the total as DRE (this is the same percentage as that in the 2017 Nishinoshima activity; Kaneko et al. 2019b), the total volume was estimated to be  $469,000 \text{ m}^3$ . The effusion of this lava flow was assumed to have started around 12:00 JST on 5 December, and continued for 23.3 h (0.97 days) until the observation time for the ALOS-2 image. In fact, we could not specify the exact timing of the start of lava effusion from the thermal anomaly because of clouds (Fig. 3). Small thermal anomalies were observed around 15:00 in the time-series variation of the 3.9  $\mu\text{m}$  images (“P” in Fig. 3b), which suggested that lava effusion had started at least by this time. In addition, it was reported that infrasound waves and earthquakes detected in the



island increased around 12:00 on the same day (Ohminato 2020). We used these observations to assume that lava effusion had started at 12:00 on 5 December. Thus, the effusion rate was calculated to be  $0.48 \times 10^6 \text{ m}^3 \text{ day}^{-1}$ . This value agrees with the effusion-rate estimate based on the Himawari-8 observations ( $0.50 \times 10^6 \text{ m}^3 \text{ day}^{-1}$ ).

#### Evaluation of improvement in simulation results

To evaluate how the “onsite effusion rate” obtained by Himawari-8 imaging could improve the prediction of the location of hazardous areas, we compared the simulation results for the lava-flow distribution with two different input parameters: a case with an estimated “onsite effusion rate” of  $0.47 \times 10^6 \text{ m}^3 \text{ day}^{-1}$  (93% of  $0.50 \times 10^6 \text{ m}^3 \text{ day}^{-1}$ ; here we assumed that 7% of the total effusion rate was consumed by pyroclastic

cone building) and a case with the average value of the 2013–2015 eruption. We used the simulation algorithm developed by Ishihara et al. (1990) and the digital elevation model built by the Geospatial Information Authority of Japan (GSI) (based on aerial photographs taken in December 2018; GSI Website). The eruption duration was set to 23.3 h, which was the same period between the start of effusion and the acquisition time of the ALOS-2 image (Fig. 3a). The viscosity, a temperature-dependent factor, was assumed to change with a decrease in temperature as 13,200 Pa s at 1080 °C and 100,000 Pa s at 1000 °C in the lava-flow process. These viscosity values are within the range of those estimated in the 2013–2015 Nishinoshima activity ( $10^4$ – $10^6$  Pa s) based on the morphological method (Maeno et al. 2016). We do not know the composition of the lava effused in the initial stage of the December 2019 activity because the subsequent lava flows buried it. The 1973 lava at Nishinoshima (with the lowest  $\text{SiO}_2$  content among the previous activities on this island) was chosen as a reference for the simulation, considering the decreasing trend of  $\text{SiO}_2$  content in the lava over time since 2013 (Maeno et al. 2018). The former viscosity (13,200 Pa s) matches the value at the same temperature inferred from the composition of the 1973 lava based on the magma model of Giordano et al. (2008). The temperature (1080 °C) was assumed with reference to that of the lava in the 2013–2015 (1060–1090 °C; Maeno et al. 2016) and 2017 Nishinoshima activities, and agrees with the median temperature estimated from volcanic ash from the 2020 Nishinoshima activity. Although the latter viscosity (100,000 Pa s) is slightly lower than the value estimated by the same model, it is considered realistic because lava samples from the 2013–2015 and 2017 Nishinoshima eruptions contain a certain amount of relatively large deformed bubbles ( $\sim 2$ – $3$  mm) caused by degassing of magma. These bubbles could have reduced the viscosity, and the same thing probably occurred during this activity. The effusing vent was placed at the eastern base of the pyroclastic cone (Fig. 4a).

The results are shown in Fig. 4b. About 23 h after the effusion, the lava flowed eastwards about 720–730 m from the effusing vent, and the simulated distribution is almost in agreement with the actual lava flow (Fig. 4a), suggesting that using the estimated effusion rate as the input parameter is appropriate. Figure 4c shows the results of simulations assuming the effusion rate is  $0.20 \times 10^6 \text{ m}^3 \text{ day}^{-1}$ —the average effusion rate for the 2013–2015 activity (Maeno et al. 2016). The distribution of the lava flow is much smaller than the actual distribution. These results reconfirm the importance of using the

value estimated based on actual observations for better hazard area mapping.

### Concluding remarks

To estimate the effusion rate for eruptions of low-viscosity lava, we examined its relationship with the thermal anomaly observed at 1.6  $\mu\text{m}$  by Himawari-8 in the 2017 Nishinoshima activity and confirmed that there was a very high positive correlation between these two parameters. We proposed a simple empirical method for estimating the lava-effusion rate based on a linear-regression equation obtained here. Data from the 2015 Raung activity (a large-scale effusive eruption of low-viscosity lava) suggested that the relationship was applicable up to a level of  $\sim 2 \times 10^6 \text{ m}^3 \text{ day}^{-1}$ , as these data were arranged along the extension of this regression line. We applied this method to the initial stage of the December 2019 Nishinoshima activity and estimated the lava-effusion rate to be  $0.50 \times 10^6 \text{ m}^3 \text{ day}^{-1}$ . This estimated value was concordant with the value obtained with the topographic method using an ALOS-2 image ( $0.48 \times 10^6 \text{ m}^3 \text{ day}^{-1}$ ). Further, we simulated the extent of hazard areas from the initial lava flow and compared cases using the effusion rate obtained here and the average effusion rate for the 2013–2015 eruptions. The former distribution was close to the actual distribution, while the latter was much smaller. These results showed the importance of using the value estimated based on actual observations.

For enhancing the application of this method, it is desirable to collect and examine the magma temperature, the rheological properties, the composition, and the slope inclination for various types of effusive eruptions, such as an activity with highly viscous lava forming a lava dome, and not just the low-viscosity lava flows discussed here (e.g., Coppola et al. 2013; Harris et al. 2007). In that process, in addition to the actual data, investigation using simulation software for lava flows will be useful for a systematic understanding of the relationship between the eruption rate and thermal anomalies under various conditions.

It is possible to apply the technique developed here to observations using different satellite instruments. Images with a pixel size smaller than that of Himawari-8 may need to use multiple pixels for observation. Further, we can also use MIR images instead of the 1.6- $\mu\text{m}$  images; however, in that case, we should note that the values obtained are time-averaged discharge rates, and also, ambient variation needs to be considered. When using images from polar-orbiting satellites, such as the Moderate-resolution Imaging Spectroradiometer (MODIS), it will be difficult to obtain the high-density temporal

variation of effusion rate, as the observation frequency is much lower (every 1–2 days) than that of Himawari-8.

The simple empirical method for estimating the lava-effusion rate that we developed here can be a key element for establishing a real-time monitoring and simulation system to precisely predict hazardous areas created by lava flows. Usually, we can obtain the latest Himawari-8 image about 2 h after observation by the satellite using the real-time observation system we developed (<http://vrsserv.eri.u-tokyo.ac.jp/realvolc>). The calculation time for the lava-flow simulation for the examples shown in Fig. 4b, c was about 3 h on a standard-performance PC (Mac mini Core i7, 3.2 GHz). The simple empirical method we developed enabled rapid estimation of the onsite lava-effusion rate by simply using a regression equation, such as Eq. (2). If we can build a real-time processing system linking Himawari-8 observations to the rapid effusion-rate estimation and lava-flow simulation using a high-performance PC, we will be able to precisely predict the hazardous areas using the onsite lava-effusion rate within several hours or less after the satellite observation. When an effusive eruption occurs at a volcano near residential areas, rapid estimation of the effusion rate using the data from Himawari-8 will be extremely useful for hazard management, such as considering evacuation plans.

### Abbreviations

ALOS-2: Advanced Land Observing Satellite 2; DRE: Dense-rock equivalent; GSI: Geospatial Information Authority of Japan; JMA: Japan Meteorological Agency; MIR: Mid-wave infrared; MODIS: Moderate-resolution Imaging Spectroradiometer; MODTRAN: Moderate-resolution model for LOWTRAN 7; R1.6Mx: Spectral radiance of the pixel showing the maximum value in the heat source area in 1.6- $\mu\text{m}$  images; SWIR: Shortwave infrared; TIR: Thermal infrared.

### Acknowledgments

We thank K. Murata of the NICT Science Cloud for providing Himawari-8 data; JAXA/EORC for providing the ALOS-2 image; T. Ohminato of the Earthquake Research Institute, The University of Tokyo, for giving information on the initiation time of the lava effusion; and R. Ohno for data processing.

### Authors' Contributions

Conceptualization, T.K. and T.F.; methodology; software, A.Y.; writing—original draft preparation, T.K.; writing—review and editing, T.K. and A.Y.; supervision, T.F. All authors read and approved the final manuscript.

### Funding

This work was supported by a Grant-in-Aid for Scientific Research from the Japan Society for the Promotion of Science, Kakenhi C (Grant No. 19K04011 to TK), the Cross-ministerial Strategic Innovation Promotion Program II—SIP II (Enhancement of Societal Resiliency against Natural Disasters), and the Earthquake and Volcano Hazards Observation and Research Program of the Ministry of Education, Culture, Sports, Science and Technology of Japan (No. ERI\_07).

### Availability of data and materials

This paper is based on published data that are identified in the references. The Himawari-8 images used in this study are available from the Himawari project website, <https://sc-web.nict.go.jp/himawari/himawari-archive.html>, developed by the NICT Science Cloud.



# Ethics approval and consent to participate

Not applicable.

# Consent for publication

Not applicable.

# Competing interests

The authors declare no conflict of interest.

# Author details

<sup>1</sup> Earthquake Research Institute, The University of Tokyo, 1-1-1 Yayoi, Bunkyo-ku, Tokyo 113-0032, Japan. <sup>2</sup> Mount Fuji Research Institute, 5597-1 Kenmarubi, Kamiyoshida, Fujiyoshida, Yamanashi 403-0005, Japan.

Received: 4 October 2020 Accepted: 28 January 2021

Published online: 07 February 2021

# References

- Berk A, Bernstein LS, Robertson DC (1989) MODTRAN: a moderate resolution model for LOWTRAN 7. Tech Rep, GL-TR-89-0122, Geophys Lab, AFSC, Hanscom AFB, MA. <https://apps.dtic.mil/dtic/tr/fulltext/u2/a214337.pdf>. Accessed 3 Sept 2020
- Coppola D, Laiolo M, Piscopo D, Cigolini C (2013) Rheological control on the radiant density of active lava flows and domes. *J Volcanol Geotherm Res* 249:39–48. <https://doi.org/10.1016/j.jvolgeores.2012.09.005>
- Coppola D, Barsotti S, Cigolini C, Laiolo M, Pfeiffer MA, Ripepe M (2019) Monitoring the time-averaged discharge rates, volumes and emplacement style of large lava flows by using MIROVA system: the case of the 2014–2015 eruption at Holuhraun (Iceland). *Ann Geophys* 62:VO221. <https://doi.org/10.4401/ag-7749>
- Crisp J, Bologna S (1990) A model for lava flows with two thermal components. *J Geophys Res* 95(B2):1255–1270. <https://doi.org/10.1029/JB095iB02p01255>
- Dragonì M, Tallarico A (2009) Assumptions in the evaluation of lava effusion rates from heat radiation. *J Geophys Lett* 36:1–5. <https://doi.org/10.1029/2009GL037411>
- Garel F, Kaminski E, Tait S, Limare A (2013) The influence of wind on the estimation of lava effusion rate from thermal remote-sensing. *J Volcanol Geotherm Res* 264:223–230. <https://doi.org/10.1016/j.jvolgeores.2013.08.006>
- Giordano D, Russell JK, Dingwell DB (2008) Viscosity of magmatic liquids: a model. *Earth Planet Sci Lett* 271:123–134. <https://doi.org/10.1016/j.epsl.2008.03.038>
- GSI Website: <https://www.gsi.go.jp/gyoumu/gyoumu41000.html>. Accessed 3 Sept 2020
- Harris AJL (2013) Thermal remote sensing of active volcanoes, a user's manual. Cambridge University Press, Cambridge
- Harris AJL, Blake S, Rothery DA, Stevens NF (1997) A chronology of the 1991 to 1993 Mount Etna eruption using advanced very high resolution radiometer data: Implications for real-time thermal volcano monitoring. *J Geophys Lett* 102:7985–8003. <https://doi.org/10.1029/96JB03388>
- Harris AJL, Bologna SM (2009) Lava discharge rates from satellite-measured heat flux. *J Geophys Res* 36:L19302 (1–5). <https://doi.org/10.1029/2009GL039717>
- Harris AJL, Dehn J, Calvari S (2007) Lava effusion rate definition and measurement: a review. *Bull Volcanol* 70:1–22. <https://doi.org/10.1007/s00445-007-0120-y>
- Ishihara K, Iguchi M, Kamo K (1990) Numerical simulation of lava flows on some volcanoes in Japan. In: Fink JH (ed) *Lava Flows and domes*, IAVCEI Proc Volcanol, 2. Springer, Berlin, Heidelberg
- JMA (2017) Himawari-8/9 Himawari standard data user's guide version 1.3. [https://www.data.jma.go.jp/mscweb/en/himawari89/space\\_segment/hsd\\_sample/HS\\_D\\_users\\_guide\\_en\\_v13.pdf](https://www.data.jma.go.jp/mscweb/en/himawari89/space_segment/hsd_sample/HS_D_users_guide_en_v13.pdf). Accessed 3 Sept 2020
- Kaneko T, Maeno F, Yasuda A (2019a) Observation of the eruption sequence and formation process of a temporary lava lake during the June–August 2015 Mt. Raung eruption, Indonesia, using high-resolution and high-frequency satellite image datasets. *J Volcanol Geotherm Res* 377:17–32. <https://doi.org/10.1016/j.jvolgeores.2019.03.016>
- Kaneko T, Maeno F, Yasuda A, Takeo M, Takasaki K (2019b) The 2017 Nishinoshima eruption: combined analysis using Himawari-8 and multiple high-resolution satellite images. *Earth Planets Space* 71:140. <https://doi.org/10.1186/s40623-019-1121-8>
- Kaneko T, Takasaki K, Maeno F, Wooster MJ, Yasuda A (2018a) Himawari-8 infrared observations of the June–August 2015 Mt Raung eruption, Indonesia. *Earth Planets Space* 70:89. <https://doi.org/10.1186/s40623-018-0858-9>
- Kaneko T, Wooster MJ (1999) Landsat infrared analysis of fumarole activity at Unzen volcano: time-series comparison with gas and magma fluxes. *J Volcanol Geotherm Res* 89:57–64. [https://doi.org/10.1016/S0377-0273\(98\)00122-X](https://doi.org/10.1016/S0377-0273(98)00122-X)
- Kaneko T, Wooster MJ, Nakada S (2002) Exogenous and endogenous growth of the Unzen lava dome examined by satellite infrared image analysis. *J Volcanol Geotherm Res* 116:151–160. [https://doi.org/10.1016/S0377-0273\(02\)00216-0](https://doi.org/10.1016/S0377-0273(02)00216-0)
- Kaneko T, Yasuda A, Yoshizaki Y, Takasaki K, Honda Y (2018b) Pseudo-thermal anomalies in the shortwave infrared bands of the Himawari-8 AHI and their correction for volcano thermal observation. *Earth Planets Space* 70:175. <https://doi.org/10.1186/s40623-018-0946-x>
- Kilburn CRJ, Pinkerton H, Wilson L (1995) Forecasting the behaviour of lava flows. In: McGuire B, Kilburn CRJ, Murray J (eds) *Monitoring active volcanoes: strategies, procedure and techniques*. UCL Press, London, pp 346–368
- Llewellyn EW, Manga M (2005) Bubble suspension rheology and implications for conduit flow. *J Volcanol Geotherm Res* 143:205–217. <https://doi.org/10.1016/j.jvolgeores.2004.09.018>
- Maeno F, Nakada S, Kaneko T (2016) Morphological evolution of a new volcanic islet sustained by compound lava flows. *Geology* 44(4):259–262. <https://doi.org/10.1130/G37461.1>
- Maeno F, Nakano S, Yoshimoto M, Ohminato T, Watanabe A, Kawakami K, Chida T, Takeo M (2017) First landing and survey of a new volcanic island: nishinoshima. *J Geograp* 126(1): N1–13. (in Japanese) <http://journal.geog.or.jp/images/articles/126-1/N1.pdf>. Accessed 3 Sept 2020
- Maeno F, Yasuda A, Nakano S, Yoshimoto M, Ohminato T, Watanabe A, Kaneko T, Nakada S, Takeo M (2018) Formation process of a new volcanic island at Nishinoshima, Ogasawara, Japan, inferred from eruptive products. *J Advance Mari Sci Tech Soc* 24: 35–44. (in Japanese with English abstract) [https://www.jstage.jst.go.jp/article/amstec/24/1/24\\_35/\\_pdf/-char/ja](https://www.jstage.jst.go.jp/article/amstec/24/1/24_35/_pdf/-char/ja). Accessed 3 Sept 2020
- Miyamoto H, Sasaki S (1998) Numerical simulations of flood basalt lava flows: Roles of parameters on lava flow morphologies. *J Geophys Res* 103:27489–27502. <https://doi.org/10.1029/98JB00438>
- Nakada S, Miyake Y, Sato H, Oshima O, Fujinawa A (1995) Endogenous growth of dacite dome at Unzen volcano (Japan), 1993–1994. *Geology* 23(2):157–160. [https://doi.org/10.1130/0091-7613\(1995\)023%3c0157:EGODDA%3e2.3.CO;2](https://doi.org/10.1130/0091-7613(1995)023%3c0157:EGODDA%3e2.3.CO;2)
- Nakada S, Shimizu H, Ohta K (1999) Overview of 1990–1995 eruptions at Unzen Volcano. *J Volcanol Geotherm Res* 89:1–22. [https://doi.org/10.1016/S0377-0273\(98\)00118-8](https://doi.org/10.1016/S0377-0273(98)00118-8)
- NASA (2019) GOES-R series data book, revision A. <https://www.goes-r.gov/downloads/resources/documents/GOES-RSeriesDataBook.pdf>. Accessed 3 Sept 2020
- Ohminato T (2020) The 2019–20 Nishinoshima activity: seismic and infrasound observation. <http://www.eri.u-tokyo.ac.jp/2020/07/07/nishinoshima-5/>. (in Japanese) Accessed 3 Sept 2020
- Pieri DC, Bologna SM (1986) Eruption rate, area, and length relationships for some Hawaiian lava flows. *J Volcanol Geotherm Res* 30:29–45. [https://doi.org/10.1016/0377-0273\(86\)90066-1](https://doi.org/10.1016/0377-0273(86)90066-1)
- Rogic N, Cappello A, Ferrucci F (2019) Role of emissivity in lava flow 'Distance-to-Run' estimates from satellite-based volcano monitoring. *Remote Sens*. <https://doi.org/10.3390/rs11060662>
- Swanson DA, Dzurisin D, Holcomb RT, Iwatsubo EY, Chadwick Jr WW, Casadevall TJ, Ewert JW, Heliker CC (1987) Growth of the lava dome at Mount St. Helens, Washington (USA), 1981–1983. In: Fink J (ed) *The emplacement of silicic domes and lava flows*. *Geol Soc Am Spec Pap* 212: 1–16. <https://doi.org/10.1130/SPE212-p1>
- Wadge G (1981) The variation of magma discharge during basaltic eruption. *J Volcanol Geotherm Res* 11:139–168. [https://doi.org/10.1016/0377-0273\(81\)90020-2](https://doi.org/10.1016/0377-0273(81)90020-2)
- Walker GPL (1973) Lengths of lava flows. *Phil Trans R Soc Lond A* 274:107–118
- Walter LS, Salisbury JW (1989) Spectral characterization of igneous rocks in the 8- to 12-μm region. *J Geophys Res* 94:9203–9213. <https://doi.org/10.1029/JB094iB07p09203>

- Wooster MJ, Kaneko T (1998) Satellite thermal analysis of lava dome effusion rate at Unzen volcano, Japan. *J Geophys Res* 103:20935–20947. <https://doi.org/10.1029/97JB03392>
- Wooster MJ, Rothery DA (1997) Thermal monitoring of Lascar volcano, Chile, using infrared data from the along-track scanning radiometer: a 1992–1995 time series. *Bull Volcanol* 58:566–579. <https://doi.org/10.1007/s004450050163>
- Wooster MJ, Zhukov B, Oertel D (2003) Fire radiative energy for quantitative study of biomass burning: derivation from the BIRD experimental satellite and comparison to MODIS fire products. *Remote Sens Environ* 86:83–107. [https://doi.org/10.1016/S0034-4257\(03\)00070-1](https://doi.org/10.1016/S0034-4257(03)00070-1)
- Wright R, Blake S, Harris AJL, Rothery DA (2001) A simple explanation for the space-based calculation of lava eruption rates. *Earth Planet Sci Lett* 192:223–233. [https://doi.org/10.1016/S0012-821X\(01\)00443-5](https://doi.org/10.1016/S0012-821X(01)00443-5)
- Yamashita S, Miyamoto K (2009) Basic studies on influence of the slab layer on cooling of lava flows. Abstract of 2009 JSCE Annual Meeting, CS9–001. [http://www.jsce.or.jp/event/conf/abstract/2009/pdf/01\\_oral/O3-18.pdf](http://www.jsce.or.jp/event/conf/abstract/2009/pdf/01_oral/O3-18.pdf). (in Japanese) Accessed 3 Sept 2020

# Publisher's Note

Springer Nature remains neutral with regard to jurisdictional claims in published maps and institutional affiliations.

**Submit your manuscript to a SpringerOpen<sup>®</sup> journal and benefit from:**

- Convenient online submission
- Rigorous peer review
- Open access: articles freely available online
- High visibility within the field
- Retaining the copyright to your article

---

Submit your next manuscript at ► [springeropen.com](https://www.springeropen.com)